

neonSoilFlux: An R Package for Continuous Sensor-Based Estimation of Soil CO₂ Fluxes

John Zobitz¹ Edward Ayres² Zoey Werbin³ Ridwan Abdi¹

⁴ Natalie Ashburner-Wright⁵ Lillian Brown⁵

⁵ Ryan Frink-Sobierajski⁵ Lajntxiag Lee¹ Dijonë Mehmeti¹

⁶ Christina Tran⁵ Ly Xiong¹ Naupaka Zimmerman^{4,5}

⁷ ¹ Augsburg University, 2211 Riverside Avenue, Minneapolis, MN 55454

⁸ ² National Ecological Observatory Network, Battelle, 1685 38th Street, Suite 100, Boulder,
⁹ CO 80301

¹⁰ ³ Boston University, 5 Cummington Street, Boston, MA 02215

¹¹ ⁴ University of Kansas, 1450 Jayhawk Boulevard, Lawrence, KS 66045

¹² ⁵ University of San Francisco, 2130 Fulton Street, San Francisco, CA 94117

13 Acknowledgments

¹⁴ John Zobitz acknowledges Kathleen O'Rourke for code development. Naupaka Zimmerman
¹⁵ thanks technical staff at USF for support with field gear assembly and shipping. We thank the
¹⁶ NEON field staff and assignable assets teams for facilitating each of the six NEON site visits.

¹⁷ We are grateful to LI-COR technical staff for helpful discussions about optimal soil chamber
¹⁸ sampling methods. This work was supported by NSF DEB grant #2017829 awarded to John
¹⁹ Zobitz, and NSF DEB grant #2017860 awarded to Naupaka Zimmerman. This material is
²⁰ based in part upon work supported by the National Ecological Observatory Network (NEON),
²¹ a program sponsored by the U.S. National Science Foundation (NSF) and operated under
²² cooperative agreement by Battelle. We also thank the reviewers and subject editor for their
²³ constructive feedback.

²⁴ **Conflict of Interest Statements**

²⁵ None of the authors have a financial, personal, or professional conflict of interest related to
²⁶ this work.

²⁷ **Author Contributions**

²⁸ Conceptualization: John Zobitz, Naupaka Zimmerman; Methodology: Edward Ayres, John
²⁹ Zobitz, Naupaka Zimmerman; Software: John Zobitz, Naupaka Zimmerman, Zoey Werbin,
³⁰ Edward Ayres, Dijonë Mehmeti, Ridwan Abdi, Ly Xiong, Lajntxiag Lee; Validation: John
³¹ Zobitz, Naupaka Zimmerman; Formal Analysis: John Zobitz, Naupaka Zimmerman, Dijonë
³² Mehmeti, Ridwan Abdi, Ly Xiong, Lajntxiag Lee; Investigation: John Zobitz, Naupaka Zimmerman,
³³ Ryan Frink-Sobierajski, Christina Tran, Natalie Ashburner-Wright, Lillian Brown;
³⁴ Resources: John Zobitz, Naupaka Zimmerman; Data curation: John Zobitz, Naupaka Zimmerman,
³⁵ Dijonë Mehmeti, Ly Xiong; Writing – original draft: John Zobitz, Naupaka Zimmerman;
³⁶ Writing – review and editing: John Zobitz, Naupaka Zimmerman, Zoey Werbin, Edward Ayres,
³⁷ Christina Tran, Dijonë Mehmeti, Ly Xiong; Visualization: John Zobitz, Naupaka Zimmerman,

³⁸ Dijonë Mehmeti, Ridwan Abdi, Ly Xiong; Supervision: John Zobitz, Naupaka Zimmerman;
³⁹ Project Administration: John Zobitz, Naupaka Zimmerman; Funding Acquisition: John Zob-
⁴⁰ itz, Naupaka Zimmerman.

⁴¹ **Data Availability**

⁴² Data available via <https://doi.org/10.5281/zenodo.17516319> (Zobitz & Zimmerman, 2025).
⁴³ Field-collected data, `neonSoilFlux` calculated outputs, and manuscript-generating code are
⁴⁴ provided within this repository.

45 **1 Abstract**

- 46 1. Accurate quantification of soil carbon fluxes is essential to reduce uncertainty in esti-
47 mates of the terrestrial carbon sink. However, these fluxes vary over time and across
48 ecosystem types and so it can be difficult to estimate them accurately across large scales.
49 The flux gradient method estimates soil carbon fluxes using co-located measurements of
50 soil CO₂ concentration, soil temperature, soil moisture, and other soil properties. The
51 National Ecological Observatory Network (NEON) provides such data across 20 ecocli-
52 climatic domains spanning the continental U.S., Puerto Rico, Alaska, and Hawai‘i.
- 53 2. We present an R software package (`neonSoilFlux`) that acquires soil environmental data
54 to compute half-hourly soil carbon fluxes for each soil replicate plot at a given terrestrial
55 NEON site. To assess the computed fluxes, we visited six focal NEON sites and measured
56 soil carbon fluxes using a closed-dynamic chamber approach.
- 57 3. Outputs from the `neonSoilFlux` showed agreement with measured fluxes (R^2 between
58 measured and `neonSoilFlux` outputs ranging from 0.04 to 0.81 depending on calculation
59 method used); measured outputs generally fell within the range of calculated uncertain-
60 ties from the gradient method. Calculated fluxes from `neonSoilFlux` aggregated to the
61 daily scale exhibited expected site-specific seasonal patterns.
- 62 4. While the flux gradient method is broadly effective, its accuracy is highly sensitive to
63 site-specific inputs, including the extent to which gap-filling techniques are used to in-
64 terpolate missing sensor data and to estimates of soil diffusivity and moisture content.
65 Future refinement and validation of `neonSoilFlux` outputs can contribute to existing
66 databases of soil carbon flux measurements, providing near real-time estimates of a crit-
67 ical component of the terrestrial carbon cycle.

⁶⁸ **1.1 Keywords**

⁶⁹ Soil carbon, carbon dioxide, flux gradient, carbon cycle, field validation, soil respiration, ecosys-
⁷⁰ tem variability, diffusion

⁷¹ **2 Data for peer review**

⁷² Anonymous field-collected data, `neonSoilFlux` calculated outputs, and manuscript-generating
⁷³ code for peer review are provided as supplemental files. An anonymous link for peer-review
⁷⁴ is here: <https://doi.org/10.5281/zenodo.1695117>. This will be made publicly available upon
⁷⁵ publication.

⁷⁶ **3 Introduction**

⁷⁷ Soils contain the planet's largest reservoir of terrestrial carbon (Jobbágy & Jackson, 2000). A
⁷⁸ critical component of this reservoir is soil organic matter, the accumulation of which is influ-
⁷⁹ enced by biotic factors such as above-ground plant inputs (Jackson et al., 2017). These inputs
⁸⁰ in turn are influenced by environmental factors such as growing season length, temperature,
⁸¹ and moisture (Desai et al., 2022), which also affect the breakdown of soil organic matter and its
⁸² return to the atmosphere. Across heterogeneous terrestrial landscapes, the interplay between
⁸³ these biotic and abiotic factors influence the size of the soil contribution to the terrestrial
⁸⁴ carbon sink (Friedlingstein et al., 2025). However, the heterogeneity of these processes across
⁸⁵ diverse ecosystems in the context of rapid environmental change leads to large uncertainty
⁸⁶ about the magnitude of this sink in the future, and thus there remains a pressing need to
⁸⁷ quantify changes in soil carbon pools and fluxes across scales.

88 Ecological observation networks such as the United States' National Ecological Observatory
89 Network (NEON) and others (e.g. the globally-distributed FLUXNET or the European Inte-
90 grated Carbon Observation System) present a significant advancement in the nearly continuous
91 observation of biogeochemical processes at the continental scale. Notably, at 47 terrestrial sites
92 across the continental United States that span 20 ecoclimatic domains, NEON provides half-
93 hourly measurements of soil CO₂ concentration, temperature, and moisture at different vertical
94 depths. Each of these NEON sites also encompasses measurements of the cumulative sum of all
95 ecosystem carbon fluxes in an airshed using the eddy covariance technique (Baldocchi, 2014).
96 Soil observations provided by NEON are on the same timescale and standardized with eddy co-
97 variance measurements from FLUXNET. These types of nearly continuous observational data
98 (NEON and FLUXNET) can be used to reconcile differences between model-derived or data-
99 estimated components of ecosystem carbon flux (Jian et al., 2022; Luo et al., 2011; Phillips et
100 al., 2017; J. Shao et al., 2015; P. Shao et al., 2013; Sihl et al., 2016).

101 Estimated or observed soil carbon fluxes are a key metric for understanding change in soil
102 carbon pools over time (Bond-Lamberty et al., 2024). A soil carbon flux to the atmosphere
103 (F_S , units $\mu\text{mol m}^{-2} \text{ s}^{-1}$), represents the aggregate process of transfer of soil CO₂ to the
104 atmosphere from physical and biological processes (e.g. diffusion and respiration). Soil carbon
105 fluxes can be assumed to encompass soil carbon respiration from autotrophic or heterotrophic
106 sources (Davidson et al., 2006) and modeled with a exponential Q_{10} paradigm (Bond-Lamberty
107 et al., 2004; Chen & Tian, 2005; Hamdi et al., 2013).

108 One common method by which F_S is measured in the field is through the use of soil chambers
109 in a closed, well-mixed system (Norman et al., 1997) with headspace trace gas concentrations
110 measured with an infrared gas analyzer (IRGA). F_S can also be estimated from soil CO₂
111 measurements at different depths in the soil using the flux-gradient method (Maier & Schack-
112 Kirchner, 2014). Closed-chamber IRGA measurements, while being the most common method,

require either frequent in-person site visits or expensive and fragile automated systems. The potential of the gradient method is that fluxes can be estimated from continuous data recorded by robust solid-state sensors. The flux-gradient method is an approach that uses conservation of mass to calculate flux at a vertical soil depth z at steady state by applying Fick's law of diffusion. A simplifying assumption for the flux-gradient method is that there is no mass transfer in the other spatial dimensions x and y (Maier & Schack-Kirchner, 2014). The diffusivity profile, a key component of this calculation, varies across the soil depth as a function of soil temperature, soil volumetric water content, atmospheric air pressure, and soil bulk density (Millington & Shearer, 1971; Moldrup et al., 1999; Sallam et al., 1984).

Databases such as the Soil Respiration Database (SRDB) or the Continuous Soil Respiration Database (COSORE) add to the growing network of resources for making collected observations of soil fluxes available to other researchers (Bond-Lamberty, 2018; Bond-Lamberty et al., 2020; Bond-Lamberty & Thomson, 2010; Jian et al., 2021; Jiang et al., 2024). However, these databases currently encompass primarily direct soil measurements of fluxes (i.e. those using methods like the closed-chamber method described above). Currently, NEON provides all measurements to calculate F_S from Fick's law, but soil flux as a derived data product was descoped from the initial network launch due to budget constraints (Berenbaum et al., 2015). Deriving estimates of F_S using continuous sensor data across NEON sites using NEON data thus remains a high priority.

This study describes an R software package, `neonSoilFlux`, that computes a standardized estimate of F_S at all terrestrial NEON sites using the flux-gradient method. Using direct chamber-based field observations of soil carbon dioxide flux from a subset of terrestrial NEON sites spanning six states, we provide a direct validation of F_S from `neonSoilFlux`. While open source R software tools currently exist for processing chamber-based flux measurements (Jurasinski et al., 2022; Pedersen, 2024; Rheault et al., 2024; Wilson et al., 2024; Zhao, 2019),

138 to our knowledge this is the first package that incorporates NEON data directly.

139 Key objectives of this study are to:

- 140 1. Apply the flux-gradient method to estimate soil CO₂ flux from continuous sensor mea-
- 141 surements across six NEON sites.
- 142 2. Benchmark estimated soil carbon fluxes against field measurements (e.g. direct chamber
- 143 measurements of soil flux).
- 144 3. Identify sources of error in the flux-gradient approach across diverse sites in order to
- 145 guide future work.

146 **4 Materials and Methods**

147 **4.1 Field methods**

148 **4.1.1 Focal NEON Sites**

149 In order to acquire field data to validate model predictions of flux, we selected six terrestrial
150 NEON sites for analysis. We conducted roughly week-long field measurement campaigns at
151 these sites, which span a range of environmental gradients and terrestrial domains (Table 1).
152 SJER, SRER, and WREF were visited during May and June of 2022, and WOOD, KONZ,
153 and UNDE during May and June of 2024.

154 **4.1.2 Soil collar placement**

155 Either one (2022 sampling campaign) or two (2024 sampling campaign) PVC soil collars (20.1
156 cm inside diameter) were installed in close proximity to the permanent NEON soil sensors at

157 each site (Figure 1). As instruments in the NEON soil sensor arrays can occasionally break
158 down or stop working, the specific soil plot where we made measurements was chosen at each
159 site in consultation with NEON staff to maximize likelihood of quality soil sensor measurements
160 during the duration of the IRGA measurements. The plot selected at each site (out of the 5 in
161 each replicate array at each site) are presented in the last column of Table 1. After installation,
162 collar(s) were left to equilibrate for approximately 24 hours prior to any measurements being
163 taken.

164 **4.1.3 Infrared gas analyzer measurements of soil CO₂ flux**

165 In 2022, we then made measurements of flux on an hourly interval for 8 hours each day.
166 Measurements were taken from roughly 8 am to 4 pm, with the time interval selected to
167 capture the majority of the diurnal gradient of soil temperature each day. These measurements
168 were made using a LI-6800 infrared gas analyzer instrument (LI-COR Environmental, Lincoln,
169 NE) fitted with a soil chamber attachment (attachment 6800-09). In 2024, we again used the
170 same LI-6800 instrument, but made half-hourly measurements over an approximately 8 hour
171 period. In addition, in 2024 we also installed a second collar and used a second instrument, an
172 LI-870 CO₂ IRGA, connected to an automated robotic chamber (LI-COR chamber 8200-104)
173 controlled by an LI-8250 multiplexer to make automated measurements. The multiplexer was
174 configured to take half-hourly measurements 24 hours a day for the duration of our sampling
175 bout at each site. Each instrument was paired with a soil temperature and moisture probe
176 (Stevens HydraProbe, Stevens Water, Portland, OR) that was used to make soil temperature
177 and moisture measurements concurrent with the CO₂ flux measurements. Chamber volumes
178 were set by measuring collar offsets at each site. System checks were conducted daily for the
179 LI-6800 and weekly for the LI-8250. Instruments were factory calibrated before each field
180 season.

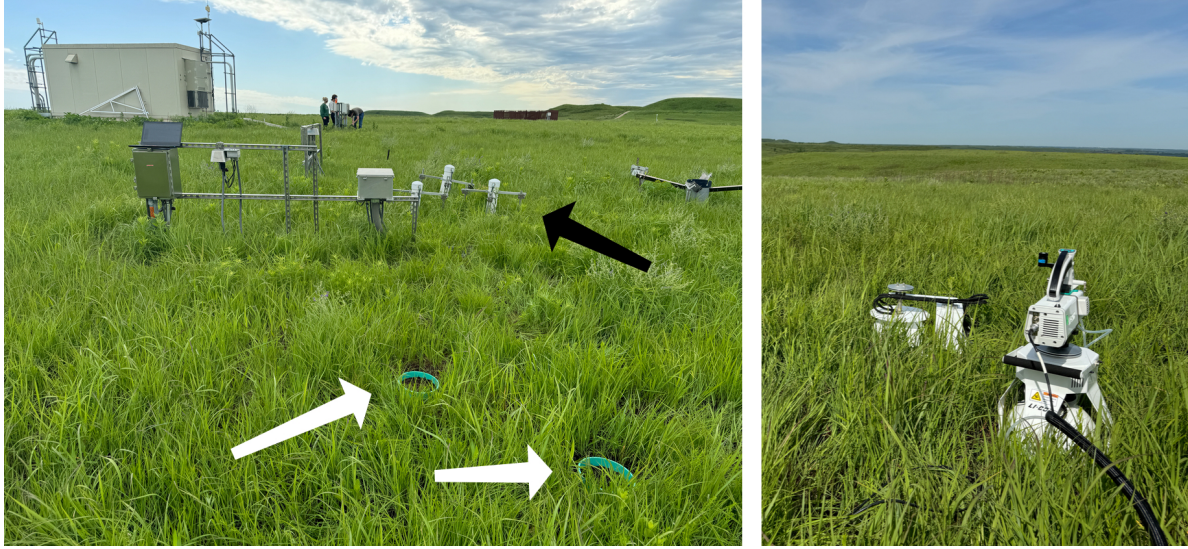


Figure 1: Spatial layout of field sampling using a closed-dynamic chamber setup at a representative NEON site (KONZ). Left image shows collars (white arrows) and permanent soil sensor installation (black arrow) and right image shows the LI-6800 (foreground) and LI-8200-104 (background) instruments placed on the collars.

Table 1: Listing of NEON sites studied for field work and analysis. Site refers to NEON site codes: Santa Rita Experimental Range (SRER), San Joaquin Experimental Range (SJER), Wind River Experimental Forest (WREF), Chase Lake National Wildlife Refuge (WOOD), Konza Prairie Biological Station (KONZ), and the University of Notre Dame Environmental Research Center (UNDE). Location is reported in decimal degrees of latitude and longitude. Other abbreviations include Mean Annual Temperature (MAT); \bar{T}_S : average soil temperature during field measurements; \bar{SWC} : average soil water content during field measurements. Dates refer to field measurement dates for each site. Plot refers to the particular location in the soil sensor array (denoted as HOR by NEON) where field measurements were made.

| Site | Location | Ecosystem | MAT | \bar{T}_S | MAP | \bar{SWC} | Dates | Plot |
|------|--------------------------|----------------------|---------|-------------|---------|-------------|------------------------|------|
| SRER | 31.91068, -110.83549 | Shrubland | 19.3 °C | 47.6 °C | 346 mm | 4.0% | May 29– June 1 2022 | 004 |
| SJER | 37.10878, -119.73228 | Oak woodland | 16.4 °C | 41.7 °C | 540 mm | 1.2% | June 1–4 2022 | 005 |
| WREF | 45.82049, -121.95191 | Evergreen forest | 9.2 °C | 15.3 °C | 2225 mm | 27.2% | June 7–9 2022 | 001 |
| WOOD | 47.1282, -99.241334 | Restored prairie | 4.9 °C | 14.9 °C | 495 mm | 14.9% | June 3–9 2024 | 001 |
| KONZ | 39.100774, -96.563075 | Tallgrass prairie | 12.4 °C | 23.4 °C | 870 mm | 23.4% | May 29– June 1 2024 | 001 |

Table 1: Listing of NEON sites studied for field work and analysis. Site refers to NEON site codes: Santa Rita Experimental Range (SRER), San Joaquin Experimental Range (SJER), Wind River Experimental Forest (WREF), Chase Lake National Wildlife Refuge (WOOD), Konza Prairie Biological Station (KONZ), and the University of Notre Dame Environmental Research Center (UNDE). Location is reported in decimal degrees of latitude and longitude. Other abbreviations include Mean Annual Temperature (MAT); \bar{T}_S : average soil temperature during field measurements; \bar{SWC} : average soil water content during field measurements. Dates refer to field measurement dates for each site. Plot refers to the particular location in the soil sensor array (denoted as HOR by NEON) where field measurements were made.

| Site | Location | Ecosystem | MAT | \bar{T}_S | MAP | \bar{SWC} | Dates | Plot |
|------|-------------------------|---------------------|--------|-------------|--------|-------------|-------------------|------|
| UNDE | 46.23391, -89.537254 | Deciduous forest | 4.3 °C | 13.0 °C | 802 mm | 13.0% | May 22–25 2024 | 004 |

181 4.1.4 Post-collection processing of field data

182 We used LI-COR SoilFluxPro software (v 5.3.1) to assess the data after collection and to inform
 183 sampling parameters. We checked appropriateness of dead band and measurement durations
 184 using built-in evaluation tools. Based on this, the deadband period was set for 30-40 seconds,
 185 depending on the site, and the measurement duration was 180 seconds with a 30 second pre-
 186 purge and a 30 second post-purge at most sites, and a 90 second pre- and post-purge at sites
 187 with higher humidity due to recent precipitation events. We also assessed the R^2 of linear and
 188 exponential model fits to measured CO₂ to verify measurement quality.

189 4.2 neonSoilFlux R package

190 We developed an R package called `neonSoilFlux` (Zobitz et al., 2024) to compute half-hourly
 191 soil carbon fluxes and uncertainties from NEON data. The objective of the `neonSoilFlux`
 192 package is a unified workflow (Figure 2) for soil data acquisition and analysis that supplements
 193 the existing `neonUtilities` data acquisition R package (Lunch et al., 2025).

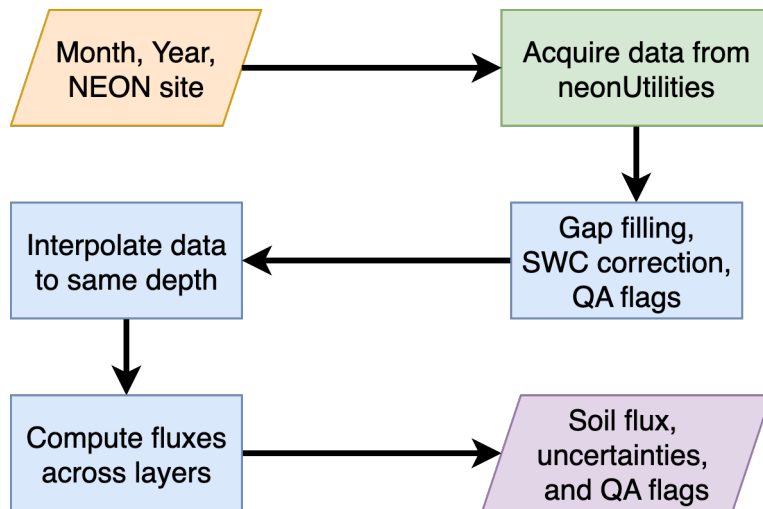


Figure 2: Diagram of `neonSoilFlux` R package. For a given month, year, and NEON site (orange parallelogram), the package acquires all relevant data to compute F_S using the `neonUtilities` R package (green rectangle). Data are gap-filled according to reported QA flags and adjusted for changes in soil water content (SWC) calibration coefficients, then interpolated to the same measurement depth before computing the soil flux, uncertainties, and final QA flags (blue rectangles). The package reports the associated soil flux, uncertainties, and quality assurance (QA) flags for the user (purple parallelogram).

At a given NEON site there are five replicate soil plots, each with measurements of soil CO_2 concentration, soil temperature, and soil moisture at different depths (Figure 3). The `neonSoilFlux` package acquires measured soil CO_2 concentration (NEON, 2024b), soil temperature (NEON, 2024d), soil water content (NEON, 2024e), barometric pressure from the nearby tower (NEON, 2024a), and soil properties (e.g. bulk density) (NEON, 2024c) from a range of different NEON data products. The static soil properties were collected by NEON staff from a nearby soil pit during initial site characterization and are assumed to be constant at each site. A soil flux calculation is computed at each replicate soil plot.

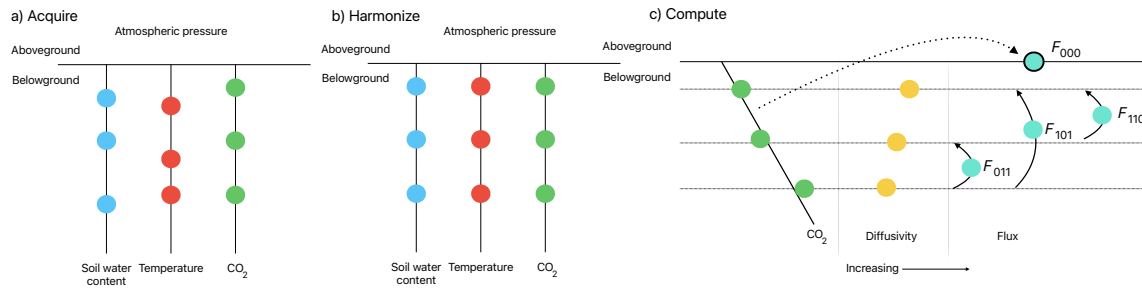


Figure 3: Model diagram of the data workflow for the `neonSoilFlux` R package. a) Acquire: Data are obtained for a given NEON location and horizontal sensor location, which includes soil water content, soil temperature, CO_2 concentration, and atmospheric pressure. All data are screened for quality assurance; if gap-filling of missing data occurs, it is flagged for the user. b) Harmonize: Any belowground data are then harmonized to the same depth as CO_2 concentrations using linear regression. c) Compute: The flux across a given depth is computed via Fick's law, denoted with F_{ijk} , where i , j , or k are either 0 or 1 denoting the layers the flux is computed across ($i = \text{closest to surface}$, $k = \text{deepest}$). F_{000} represents a flux estimate where the gradient dC/dz is the slope of a linear regression of CO_2 with depth.

The workflow to compute a value of F_S with `neonSoilFlux` consists of three primary steps, illustrated in Figure 3. First, NEON data are acquired for a given site and month via the `neonUtilities` R package (yellow parallelogram and green rectangle in Figure 2 and Panel a in Figure 3). Acquired environmental data can be exported to a comma separated value file for additional analysis. Quality assurance (QA) flags are reported as an indicator variable. Since

207 the calibration coefficients on the soil water content sensors have changed over time (NEON,
208 2024e), raw sensor measurements were back-calculated and soil-specific calibrations were ap-
209 plied following Ayres et al. (2024) to generate a consistent time series at each measurement
210 location.

211 The second step is harmonizing the data to compute soil fluxes across soil layers. This step
212 consists of three different actions (blue rectangles in Figure 2 and Panel b in Figure 3). If a
213 given observation by NEON is reported as not passing a quality assurance check, we applied
214 a gap filling method to replace that measurement with its monthly mean at that same depth
215 (Section 4.2.1). Belowground measurements of soil water and soil temperature are then inter-
216 polated to the same depth as soil CO₂ measurements. The diffusivity (Section 4.2.2) and soil
217 flux across different soil layers (Section 4.2.3) are then computed.

218 The third and final step is computing a surface soil flux through extrapolation to the sur-
219 face (purple parallelogram in Figure 2 and Panel c in Figure 3). Uncertainty on a soil flux
220 measurement is computed through quadrature. An aggregate quality assurance (QA) flag
221 for each environmental measurement is also reported, representing if any gap-filled measure-
222 ments were used in the computation of a soil flux. Within the soil flux-gradient method,
223 several different approaches can be used to derive a surface flux (Maier & Schack-Kirchner,
224 2014); the `neonSoilFlux` package reports four different possible values for soil surface flux
225 (Section 4.2.3) for each of two different methods of diffusivity estimation, for a total of eight
226 estimates of flux.

227 **4.2.1 Gap-filling routine**

228 NEON reports QA flags as binary values for each measurement and half-hourly interval. For
229 a given half-hour, if any input variable (soil CO₂ concentration, soil temperature, or soil

230 moisture) at depth z is flagged, computation of F_S is not possible. To address this, flagged
231 measurements and their uncertainties were replaced with a bootstrapped monthly mean (\bar{m})
232 and monthly standard deviation (\bar{s}) (Efron & Tibshirani, 1994).

233 For each month, depth z , and variable, we computed bootstrapped estimates of \bar{m} and \bar{s}
234 from the vectors of unflagged measurements (\mathbf{m}), reported standard errors (σ), and the 95%
235 confidence interval (ϵ , or expanded uncertainty; Farrance & Frenkel (2012)). We also defined
236 a bias vector $\mathbf{b} = \sqrt{\epsilon^2 - \sigma^2}$, which quantifies the spread of uncertainty in a given period and
237 is incorporated into \bar{m} .

238 From these, 5000 bootstrap samples were generated for \mathbf{m}, σ , and \mathbf{b} . For each sample
239 (m_k, b_k, σ_k), we generated a vector \mathbf{n} (length $N = 5000$) by drawing from a normal dis-
240 tribution with mean $m_k + b_k$ and standard deviation σ_k . The sample mean and standard
241 deviation were then computed from \mathbf{n} . The resulting distributions of sample means and
242 sample standard deviations provided the bootstrapped monthly mean (\bar{m}) and standard error
243 (\bar{s}) respectively.

244 This gap-filling procedure provides a consistent treatment across all data streams. However,
245 alternative approaches may be better suited for longer gaps (e.g., correlations with other
246 NEON measurement levels or soil plots) or for variable-specific conditions. We discuss the
247 effect of gap-filling on our results in Section 6.1.

248 **4.2.2 Soil diffusivity**

249 Soil diffusivity D_a at a given measurement depth is the product of the diffusivity in free air
250 $D_{a,0}$ ($\text{m}^2 \text{ s}^{-1}$) and the tortuosity ξ (no units) (Millington & Shearer, 1971).

251 We compute $D_{a,0}$ with Equation 1:

$$D_{a,0} = 0.0000147 \cdot \left(\frac{T_i + 273.15}{293.15} \right)^{1.75} \cdot \left(\frac{P}{101.3} \right) \quad (1)$$

252 where T_i is soil temperature ($^{\circ}\text{C}$) at depth i (NEON, 2024d) and P surface barometric pressure
 253 (kPa) (NEON, 2024a).

254 Previous studies by Sallam et al. (1984) and Tang et al. (2003) demonstrated the sensitivity
 255 of modeled F_S depending on the tortuosity model (ξ) used to compute diffusivity. At low
 256 soil water content, the choice of tortuosity model can lead to order-of-magnitude differences
 257 in D_a , which in turn affect modeled F_S . The `neonSoilFlux` package currently includes two
 258 approaches to calculate ξ , representing the range of tortuosity behavior reported in Sallam et
 259 al. (1984).

260 The first approach is the Millington-Quirk model (Millington & Shearer, 1971), in which
 261 tortuosity depends on both porosity and soil water content:

$$\xi = \frac{(\phi - SWC_i)^{10/3}}{\phi^2} \quad (2)$$

262 In Equation 2, SWC is the soil water content at depth i (NEON, 2024e) and ϕ is the porosity,
 263 which in turn is a function of soil physical properties (NEON, 2024c):

$$\phi = \left(1 - \frac{\rho_s}{\rho_m} \right) (1 - f_V) \quad (3)$$

264 In Equation 3, ρ_m is the particle density of mineral soil (2.65 g cm^{-3}), ρ_s the soil bulk density (g
 265 cm^{-3}) excluding coarse fragments greater than 2 mm (NEON, 2024c), and f_V is a site-specific
 266 value that accounts for the proportion of soil fragments between 2-20 mm. Soil fragments

267 greater than 20 mm were not estimated due to limitations in the amount of soil that can be
268 analyzed (NEON, 2024c). We assume that rock fragments contain no internal pores.

269 The Millington-Quirk model assumes ξ is modulated by the amount of fluid saturation in
270 soil pores (Millington & Shearer, 1971). In contrast, the Marshall model (Marshall, 1959)
271 expresses tortuosity as only a function of porosity ($\xi = \phi^{1.5}$), with ϕ defined from Equation
272 3. The Marshall model is independent of soil water content and assumes tortuosity is only
273 governed by soil structure. The `neonSoilFlux` package allows users to choose the tortuosity
274 model most appropriate for site-specific conditions and research goals.

275 **4.2.3 Soil flux computation**

276 We applied Fick's law (Equation 4) to compute the soil flux F_{ij} ($\mu\text{mol m}^{-2} \text{s}^{-1}$) across two
277 soil depths i and j :

$$F_{ij} = -D_a \frac{dC}{dz} \quad (4)$$

278 where D_a is the diffusivity ($\text{m}^2 \text{s}^{-1}$) and $\frac{dC}{dz}$ is the gradient of CO₂ molar concentration
279 ($\mu\text{mol m}^{-3}$, so the gradient has units of $\mu\text{mol m}^{-3} \text{m}^{-1}$). The soil surface flux is theoretically
280 defined by applying Equation 4 to measurements collected at the soil surface and directly
281 below the surface. Measurements of soil temperature, soil water content, and soil CO₂ molar
282 concentration across the soil profile allow for application of Equation 4 across different soil
283 depths. Each site had three measurement layers, so we denote the flux as a three-digit subscript
284 F_{ijk} with indicator variables i , j , and k indicate if a given layer was used (written in order of
285 increasing depth), according to the following:

- F_{000} is a surface flux estimate using the intercept of the linear regression of D_a with depth and the slope from the linear regression of CO₂ with depth (which represents $\frac{dC}{dz}$ in Fick's Law). Tang et al. (2003) used this approach to compute fluxes in an oak-grass savannah.
- F_{110} is a flux estimate across the two shallowest measurement layers.
- F_{011} is a flux estimate across the two deepest measurement layers.
- F_{101} is a flux estimate across the shallowest and deepest measurement layers.

For F_{110} , F_{011} , and F_{101} , the diffusivity used in Fick's Law is always at the deeper measurement layer. When used as a surface flux estimate we assume CO₂ remains constant above this flux depth. Uncertainty in all F_{ijk} values was quantified using quadrature (Taylor, 2022). These computed fluxes could provide the basis for additional soil flux estimates. For example, Tang et al. (2005) estimated surface flux by linearly extrapolating F_{110} and F_{011} to the soil surface.

4.3 Post processing evaluation

Following collection of field measurements and calculation of the soil fluxes from `neonSoilFlux` package, we compared measured F_S based on closed-dynamic chamber measurements with the LI-COR instruments to a given soil flux calculation from `neonSoilFlux` for each site and flux computation method and quantified the relationship statistically (R^2). Finally, for a half-hourly interval we also computed a *post hoc* diffusivity (D_a) using the LI-COR flux along with the CO₂ surface gradient reported by NEON using the measurement levels closest to the surface.

Table 2: Summary of measured soil characteristics and flux results from field measurements across six NEON sites using a LI-COR 6800 (LI-870/8250 measurements omitted to enable direct comparability) via the closed-dynamic chamber method. Numeric values for soil CO₂ flux, soil temperature, and volumetric soil water content (VSWC) are the mean and standard deviation of field measurements at each site.

| Site | Flux μmol m ⁻² s ⁻¹ | Soil temp °C | VSWC cm ³ cm ⁻³ | n |
|------|--|-----------------|--|----|
| UNDE | 2.55 ± 0.26 | 14.33 ± 0.77 | 0.33 ± 0.02 | 61 |
| WOOD | 3.02 ± 0.4 | 16.01 ± 1.54 | 0.28 ± 0.01 | 53 |
| WREF | 3.62 ± 0.3 | 15.34 ± 1.76 | 0.27 ± 0.06 | 21 |
| KONZ | 6.35 ± 0.97 | 27.28 ± 4.14 | 0.37 ± 0.01 | 44 |
| SJER | 0.94 ± 0.02 | 41.68 ± 11.22 | 0.01 ± 0.01 | 32 |
| SRER | 0.72 ± 0.09 | 47.64 ± 7.46 | 0.04 ± 0.01 | 32 |

5 Results

Concordance between modelled and measured soil CO₂ flux

The sites we visited ranged substantially in both their annual average temperature and precipitation as well as their biome type (Table 2). These differences also influenced the wide range of observed flux rates across sites.

The timeseries of the measured fluxes from the LI-COR 6800 and 870/8250 were compared to modeled soil fluxes from the `neonSoilFlux` R package (Figure 4). We also assessed year-long estimated flux time series and compared those to field measurements made at each site (Figure 5). Results are reported in local time. Where applicable, sites are displayed from left to right by increasing soil temperature (Table 1). Positive values of the flux indicate that there is a flux moving towards the surface. Overall, with the exception of SRER (discussed later) the computed fluxes determined using a variety of plausible methods spanned the field-measured fluxes, but the specific flux-gradient method that best approximated field measurements varied by site.

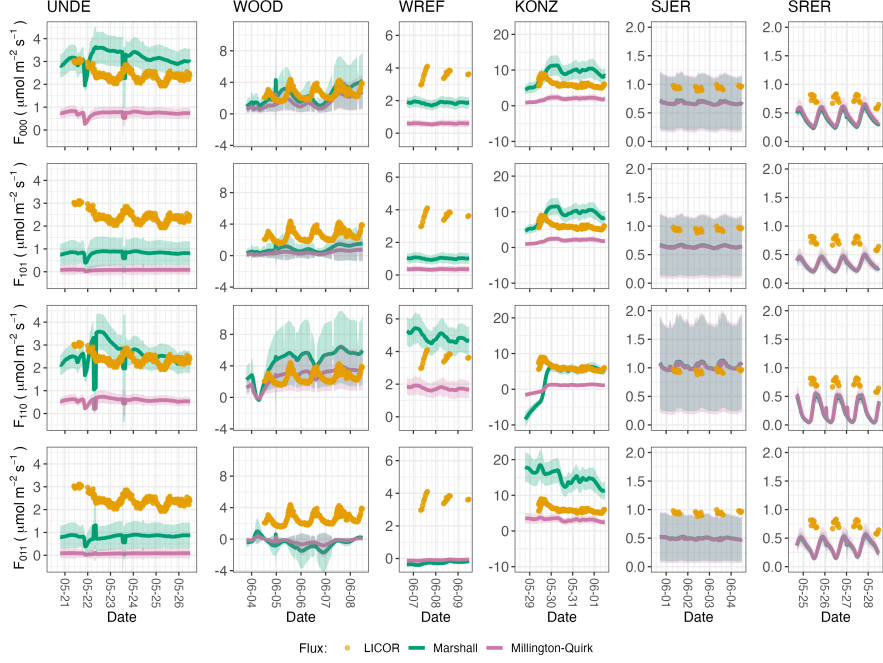


Figure 4: Timeseries of soil surface flux (F_S) from field-measured (yellow lines) and modeled soil fluxes (green or purple lines) by the `neonSoilFlux` R package. Fluxes from the `neonSoilFlux` R package are separated by the diffusivity model used (Millington-Quirk or Marshall, Section 4.2.2). Individual vertical axis labels in the first column represent the measurement levels where the flux-gradient approach is applied (Section 4.2.3). Ribbons for modeled soil fluxes represent ± 1 standard deviation. Results are reported in local time. WREF, SJER, and SRER were sampled in 2022, and UNDE, WOOD, and KONZ were sampled in 2024. Sites (columns) are arranged from left to right in terms of increasing mean annual temperature.

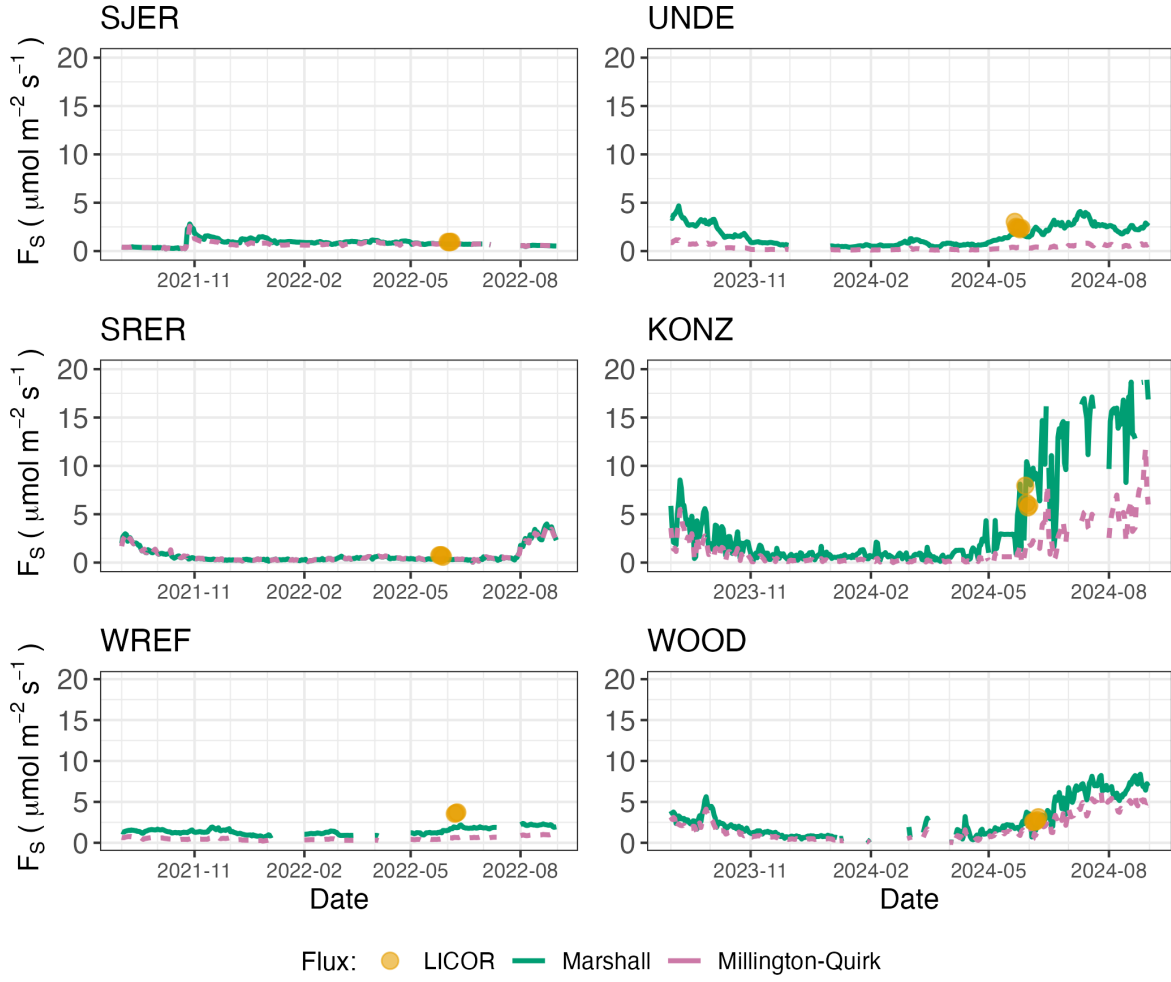


Figure 5: Timeseries of both daily-averaged field F_S (yellow circles) and daily ensemble averaged soil fluxes (average of F_{000} , F_{101} , F_{011} , F_{110} , Section 4.2.3) by the `neonSoilFlux` R package, separated by the diffusivity model used (green or purple lines, Millington-Quirk or Marshall, Section 4.2.2).

320 We calculated a statistical relationship between the various estimates of soil flux computed by
321 `neonSoilFlux` and the field-measured fluxes within daily interval periods. Statistics for these
322 comparisons are reported in Figure 6, which also shows how these fall relative to a 1:1 line.

323 **5.2 Effects of method choice on diffusivity estimates**

324 In four of six field sites, the *post hoc* D_a estimate fell roughly between the two diffusion
325 estimation methods; however this was less the case in the two driest sites, SJER and SRER
326 (Table 1), where the field estimate of diffusivity was either lower or higher than both of the
327 other methods (Figure 7).

328 **6 Discussion**

329 This study presents a unified data science workflow to efficiently process automated measure-
330 ments of belowground soil CO₂ concentrations, soil water content, and soil temperature to
331 infer estimates of soil surface CO₂ effluxes through application of Fick's Law (Equation 4).
332 Our core goals in this study were: (1) to generate estimates of soil flux from continuous soil
333 sensor data at terrestrial NEON sites using the flux-gradient method and then (2) to compare
334 those estimates to field-measured fluxes based on the closed chamber approach at six NEON
335 focal sites. We discuss our progress toward these core goals through (1) an overall evaluation
336 of the flux-gradient approach (and uncertainty calculation) and (2) site-specific evaluation of
337 differences in estimated vs measured fluxes.

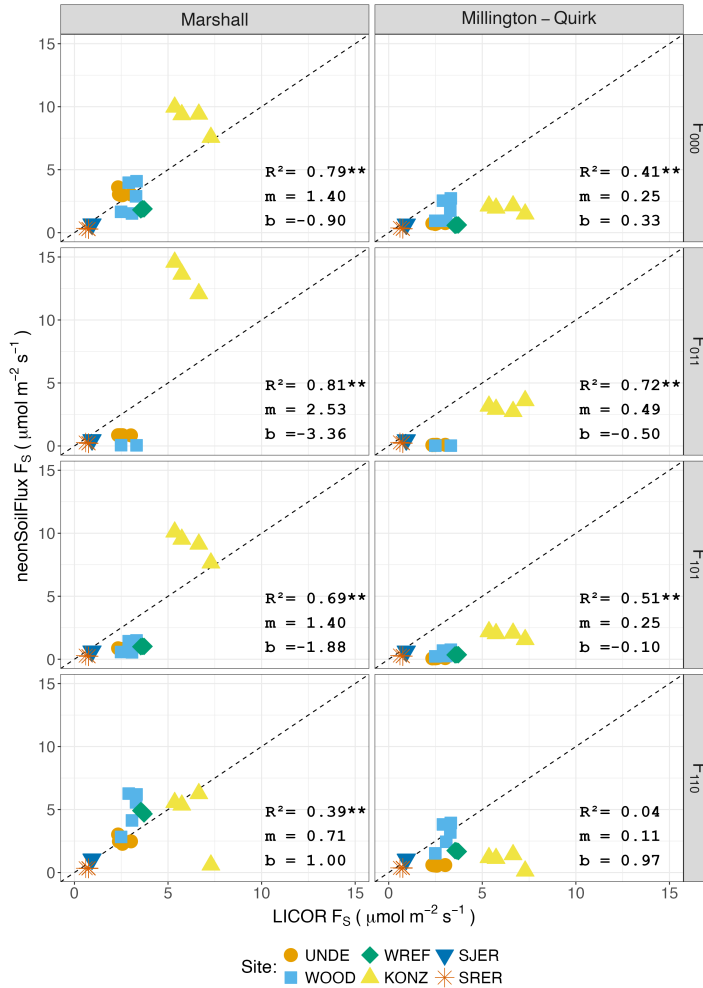


Figure 6: Statistical comparison between measured fluxes at each NEON site with fluxes reported by `neonSoilFlux` with the different flux calculation approaches and diffusivity calculations applied. Points are daily averages and LICOR F_S values are from the 6800 instrument only, for consistency. The dotted line represents a 1:1 relationship, and the reported R^2 quantifies the relationship between field-measured and `neonSoilFlux` estimated fluxes. * = significance at the 5% level, ** = significance at the 1% level. The slope (m) and intercept (b) of the linear regression between measured and modeled fluxes are also reported. The low-value outlier from KONZ in the F_{110} Marshall plot is an example of the effect of inverted CO₂ gradients causing an estimated flux to be negative, bringing down the daily mean, which later resolved as the soils dried back out.

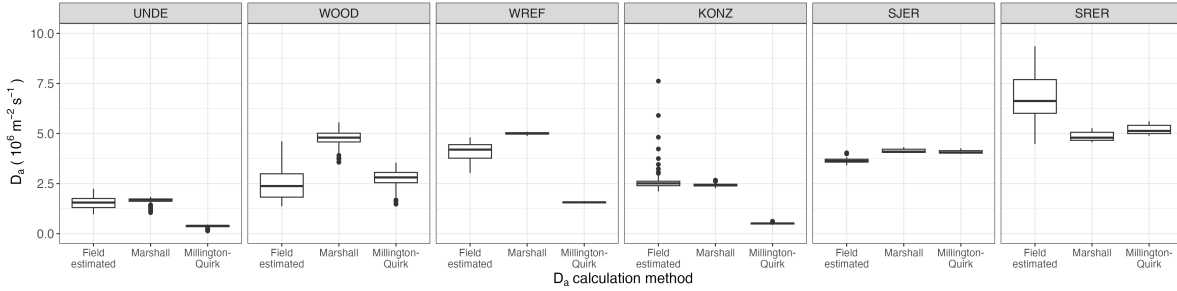


Figure 7: Distribution of diffusivity (D_a) at each study site. Values of D_a were provided by the `neonSoilFlux` package, computed from the Millington-Quirk or Marshall models (Section 4.2.2). A post-hoc estimate of diffusivity (labeled as “Field estimated”) was computed through the field measured flux (Figure 4), divided by the CO_2 gradient from the measurement levels closest to the soil surface, as reported by NEON. We only used F_S measured by the LICOR 6800 at all sites to standardize comparisons.

338 6.1 General evaluation of flux-gradient approach

339 Key assumptions of the flux-gradient approach are that CO_2 concentrations increase through-
 340 out the soil profile such that the highest concentrations are observed in the deepest layers. Ad-
 341 ditionally, field flux measurements should correlate with F_{000} because they represent surface
 342 fluxes. Periods where this gradient condition are not met generally are connected to processes
 343 that occur during soil wetting events, where more shallow soil layers produce higher concentra-
 344 tions of CO_2 due to microbial respiration pulses following rewetting. This effect is likely to be
 345 largest at sites with rich organic soils (e.g. KONZ). Based on this reasoning, in these types of
 346 situations we would *a priori* expect F_{011} (deepest layers) $\leq F_{101} \leq F_{110}$ (shallow layers) \leq
 347 F_{000} (all layers) because the previous flux estimates rely primarily on CO_2 concentrations at
 348 deeper depths, and could miss high concentrations of CO_2 produced in shallower layers.

349 When modeling soil respiration, typically a non-linear response function that also considers soil
 350 type is used (Bouma & Bryla, 2000; Yan et al., 2016, 2018). For the `neonSoilFlux` package,
 351 soil type is connected to the measurement of bulk density, which was characterized at each
 352 NEON site. This bulk density estimate is based on replicate samples collected from the site

353 megapit at a subset of soil horizons, with an estimated uncertainty of $\pm 5\%$ (NEON, 2024c).
354 Coarse fragment estimates also have very large uncertainties, but because the volume fraction
355 tends to be low in surface soils it is unlikely to contribute much additional flux uncertainty.

356 Our results suggest that the most important way to improve reliability of the flux estimate is
357 to reduce the usage of gap-filled data. The current approach to gap filling in `neonSoilFlux`
358 uses monthly mean data to gap fill—this approach decreases the ability of the estimate to be
359 responsive to short-term pulses that occur with rapid weather shifts. Four sites (KONZ, SRER,
360 WREF, and UNDE) had more than 75% of half-hourly periods with no-gap filled measurements
361 (Figure S1, Supplementary Information). Two sites (SJER and WOOD) had more than 75%
362 of half-hourly intervals with just one gap-filled measurement. The large uncertainty evident
363 in Figure 4 for estimates from WOOD and SJER are thus due in part to the gap-filling used
364 in these sites (Figure S1). While we did not need to use gap-filled measurements to compute
365 the flux at WREF, field data collection occurred following a severe rainstorm, with soils at the
366 beginning of the sampling week near their water holding capacity. In general, we recommend
367 that whenever possible, knowledge of local field conditions should influence analysis decisions
368 in addition to any QA filtering protocols in the `neonSoilFlux` package.

369 We recognize that this gap-filling approach may lead to gap-filled values that are quite different
370 from the actual values, such as an underestimate of soil moisture following rain events. Further
371 extensions of the gap filling method could use more sophisticated gap-filling routines, similar to
372 what is used for net ecosystem carbon exchange (Falge et al., 2001; Liu et al., 2023; Mariethoz et
373 al., 2015; Moffat et al., 2007; Zhang et al., 2023). Additionally, since the deepest temperature
374 and soil moisture sensors are located below the deepest CO₂ sensors at NEON sites, it is
375 possible that excluding these deeper layers from consideration prior to analysis would lead to
376 a reduced need for gap filling. Future iterations of the `neonSoilFlux` package may incorporate
377 this as an option. The current gap-filling routine provides a consistent approach that can be

378 applied to each data stream, but further work may explore alternative gap-filling approaches.

379 **6.2 Evaluation of flux-gradient approach at each site**

380 Derived results from the `neonSoilFlux` package have patterns that are broadly consistent with
381 those directly measured in the field (Figure 4 and Figure 5), even though statistical comparisons
382 between the field-measured and `neonSoilFlux` values were quite variable (e.g. R^2 ranging
383 from 0.04 to 0.81; Figure 6). One advantage of the `neonSoilFlux` package is its ability to
384 calculate fluxes across different soil depths (Figure 3), which allows for additional site-specific
385 customization. We believe the package can provide a useful baseline estimate of soil fluxes
386 that can always be complemented through additional field measurements.

387 The six locations studied provide a range of case studies that suggest different considerations
388 may apply to different sites when applying the flux-gradient method. For example, the Santa
389 Rita Experimental Range (SRER) is a desert site characterized by sandy soil, which also was
390 the location of the highest field soil temperatures that we observed (Table 2). At SRER the
391 flux across the top two layers (F_{110}) produced a pattern of soil flux most consistent with the
392 observed field data. The remaining methods F_{101} , F_{011} , or F_{000} are derived from information
393 taken from the deepest layer, which seems to have been decoupled from the surface layers both
394 in terms of temperature and CO₂ concentration. This may be a general circumstance where
395 there are large diurnal temperature extremes that rapidly change during the course of a day
396 and overnight, leading to lags in the timing of when temperature increases propagate down to
397 deeper soil layers.

398 Immediately prior to our visit to Konza Prairie (KONZ), that site that experienced a significant
399 rain event that led to wet soils that gradually dried out over the course of our time there.
400 This pulse of precipitation increased the soil CO₂ concentration at the top layer above the

401 concentrations in lower layers, leading to negative estimated flux values at the start of the
402 field sampling period. In this case it was only when the soil began to return to a baseline level
403 that the assumptions of the flux-gradient method were again met.

404 Both of the previous cases also provide context for the variable statistical comparisons between
405 field-measured soil fluxes and `neonSoilFlux` outputs (Figure 6). When considering systematic
406 deployment of this method across a measurement network, there are a number of independent
407 challenges that require careful consideration. There are clear tradeoffs between (1) accuracy
408 of modeled fluxes (defined here as closeness to field-measured F_S and the uncertainty reduc-
409 tion factor ϵ), (2) precision (which could be defined by the signal to noise ratio), and (3) the
410 choice of the diffusivity model (Section 4.2.2) or flux computation method (Section 4.2.3). A
411 sensitivity analysis (Figure S2, Supplemental Information) found that flux output uncertainty
412 was dominated by measurement uncertainty (T_S , P , SWC , or CO_2) rather than by the dif-
413 fusivity method used to compute soil flux. Notably, the F_{110} method was least sensitive to
414 measurement uncertainty likely because it best aligns with the surface chamber measurement
415 assumptions.

416 Finally, comparing the effects of different diffusivity estimation methods on the match between
417 modeled and measured fluxes (Figure 5) highlights the sensitivity of F_{ijk} to diffusivity. The
418 comparison between diffusivity estimates compared to field estimated diffusivity (Figure 7)
419 demonstrates that site parameters can dictate which measure of diffusivity is most likely to
420 be accurate in a given environmental context. Site-specific differences are largely a reflec-
421 tion of differences in soil moisture across the sites (Table 1), as not all diffusivity estimation
422 methods incorporate soil moisture equivalently. While we here have compares two approaches
423 to calculate diffusivity (the Millington-Quirk and Marshall models), it may be valuable to
424 evaluate other diffusivity models (e.g. the Moldrup model; Moldrup et al. (1999)) as well. Ul-
425 timately the choice of a particular diffusivity model could be determined based on knowledge

426 of site-specific evaluations or a set of these models could be used to generate a model ensemble
427 average as a means to trade precision for a more general approach.

428 **6.3 Recommendations for future method development**

429 The `neonSoilFlux` package provides several approaches to estimate soil flux using the gradient
430 method. We believe these approaches enable the software to be used across a range of site-
431 specific assumptions (Maier & Schack-Kirchner, 2014). We note, however, that this choice
432 can have a determinative approach on the calculated values. Ensemble averaging approaches
433 (Elshall et al., 2018; Raftery et al., 2005) may be one way to address this problem if the goal is
434 to calculate fluxes using the same method at a diverse range of different sites. Two other ideas
435 would be to apply machine learning algorithms (e.g. random forest) to generate a single flux
436 estimate across diverse sites, or using co-located estimates of net ecosystem carbon exchange
437 from eddy-flux towers to further constrain results or to assess soil flux results for plausibility
438 (Phillips et al., 2017).

439 These challenges notwithstanding, the method used here and made available in the
440 `neonSoilFlux` R package has the potential to produce nearly continuous estimates of flux
441 across all terrestrial NEON sites. These estimates are a significant improvement on available
442 approaches to constrain the portion of ecosystem respiration attributable to the soil. This,
443 in turn, also aids in our ability to understand the soil contribution to the net ecosystem flux
444 measured at these sites using the co-located eddy flux towers.

⁴⁴⁵ **7 Conclusions**

⁴⁴⁶ We used the R package `neonSoilFlux` to estimate soil CO₂ fluxes with the flux-gradient
⁴⁴⁷ method using data from buried soil sensors at NEON terrestrial sites. We compared the
⁴⁴⁸ predicted fluxes to those measured directly using a field-based closed chamber approach. Soil
⁴⁴⁹ fluxes from `neonSoilFlux` were broadly effective at producing estimates of flux comparable
⁴⁵⁰ to those measured in the field using a chamber-based technique. However `neonSoilFlux`
⁴⁵¹ outputs are quite sensitive to a number of issues, including: missing data (and thus gap-
⁴⁵² filling of input measurement datasets), the selection of soil depths used to best calculate the
⁴⁵³ gradient (which may vary between sites), and finally the choice of method used for estimating
⁴⁵⁴ soil diffusivity. The flexibility of the `neonSoilFlux` package allows the user to evaluate each
⁴⁵⁵ of these issues with site-specific knowledge and contexts. Future refinements and subsequent
⁴⁵⁶ validation of `neonSoilFlux` outputs will feed forward into evaluating soil carbon fluxes broader
⁴⁵⁷ spatial scales to enhance understanding of the ways in which soils across diverse ecosystems
⁴⁵⁸ are responding to a changing climate.

⁴⁵⁹ **Sources Cited**

- ⁴⁶⁰ Ayres, E., Reichle, R. H., Colliander, A., Cosh, M. H., & Smith, L. (2024). Validation of
⁴⁶¹ Remotely Sensed and Modeled Soil Moisture at Forested and Unforested NEON Sites.
⁴⁶² *IEEE Journal of Selected Topics in Applied Earth Observations and Remote Sensing*, 17,
⁴⁶³ 14248–14264. <https://doi.org/10.1109/JSTARS.2024.3430928>
- ⁴⁶⁴ Baldocchi, D. (2014). Measuring fluxes of trace gases and energy between ecosystems and the
⁴⁶⁵ atmosphere - the state and future of the eddy covariance method. *Global Change Biology*,
⁴⁶⁶ 20(12), 3600–3609. <https://doi.org/10.1111/gcb.12649>

- 467 Berenbaum, M. R., Carpenter, S. R., Hampton, S. E., Running, S. W., & Stanzione, D. C.
468 (2015). *Report from the NSF BIO Advisory Committee Subcommittee on NEON Scope*
469 *Impacts*.
- 470 Bond-Lamberty, B. (2018). New Techniques and Data for Understanding the Global Soil Res-
471piration Flux. *Earth's Future*, 6(9), 1176–1180. <https://doi.org/10.1029/2018EF000866>
- 472 Bond-Lamberty, B., Ballantyne, A., Berryman, E., Fluet-Chouinard, E., Jian, J., Morris, K.
473 A., Rey, A., & Vargas, R. (2024). Twenty Years of Progress, Challenges, and Opportuni-
474ties in Measuring and Understanding Soil Respiration. *Journal of Geophysical Research:*
475 *Biogeosciences*, 129(2), e2023JG007637. <https://doi.org/10.1029/2023JG007637>
- 476 Bond-Lamberty, B., Christianson, D. S., Malhotra, A., Pennington, S. C., Sihi, D., AghaK-
477 ouchak, A., Anjileli, H., Altaf Arain, M., Armesto, J. J., Ashraf, S., Ataka, M., Baldocchi,
478 D., Andrew Black, T., Buchmann, N., Carbone, M. S., Chang, S.-C., Crill, P., Curtis, P.
479 S., Davidson, E. A., ... Zou, J. (2020). COSORE: A community database for continuous
480 soil respiration and other soil-atmosphere greenhouse gas flux data. *Global Change Biology*,
481 26(12), 7268–7283. <https://doi.org/10.1111/gcb.15353>
- 482 Bond-Lamberty, B., & Thomson, A. (2010). A global database of soil respiration data. *Bio-
483 geosciences*, 7(6), 1915–1926. <https://doi.org/10.5194/bg-7-1915-2010>
- 484 Bond-Lamberty, B., Wang, C., & Gower, S. T. (2004). A global relationship between the
485 heterotrophic and autotrophic components of soil respiration? *Global Change Biology*,
486 10(10), 1756–1766. <https://doi.org/10.1111/j.1365-2486.2004.00816.x>
- 487 Bouma, T. J., & Bryla, D. R. (2000). On the assessment of root and soil respiration for soils
488 of different textures: Interactions with soil moisture contents and soil CO₂ concentrations.
489 *Plant and Soil*, 227(1), 215–221. <https://doi.org/10.1023/A:1026502414977>
- 490 Chen, H., & Tian, H.-Q. (2005). Does a General Temperature-Dependent Q10 Model of Soil
491 Respiration Exist at Biome and Global Scale? *Journal of Integrative Plant Biology*, 47(11),
492 1288–1302. <https://doi.org/10.1111/j.1744-7909.2005.00211.x>

- 493 Davidson, E. A., Janssens, I. A., & Luo, Y. (2006). On the variability of respiration in
494 terrestrial ecosystems: Moving beyond Q10. *Global Change Biology*, 12, 154–164. <https://doi.org/10.1111/j.1365-2486.2005.01065.x>
- 495
- 496 Desai, A. R., Murphy, B. A., Wiesner, S., Thom, J., Butterworth, B. J., Koupaei-Abyazani, N.,
497 Muttaqin, A., Paleri, S., Talib, A., Turner, J., Mineau, J., Merrelli, A., Stoy, P., & Davis,
498 K. (2022). Drivers of Decadal Carbon Fluxes Across Temperate Ecosystems. *Journal of*
499 *Geophysical Research: Biogeosciences*, 127(12), e2022JG007014. <https://doi.org/10.1029/2022JG007014>
- 500
- 501 Efron, B., & Tibshirani, R. J. (1994). *An Introduction to the Bootstrap*. Chapman and
502 Hall/CRC. <https://doi.org/10.1201/9780429246593>
- 503 Elshall, A. S., Ye, M., Pei, Y., Zhang, F., Niu, G.-Y., & Barron-Gafford, G. A. (2018). Relative
504 model score: A scoring rule for evaluating ensemble simulations with application to micro-
505 bial soil respiration modeling. *Stochastic Environmental Research and Risk Assessment*,
506 32(10), 2809–2819. <https://doi.org/10.1007/s00477-018-1592-3>
- 507 Falge, E., Baldocchi, D., Olson, R., Anthoni, P., Aubinet, M., Bernhofer, C., Burba, G.,
508 Ceulemans, R., Clement, R., Dolman, H., Granier, A., Gross, P., Grünwald, T., Hollinger,
509 D., Jensen, N.-O., Katul, G., Keronen, P., Kowalski, A., Lai, C. T., ... Wofsy, S. (2001).
510 Gap filling strategies for defensible annual sums of net ecosystem exchange. *Agricultural*
511 *and Forest Meteorology*, 107(1), 43–69. [https://doi.org/10.1016/S0168-1923\(00\)00225-2](https://doi.org/10.1016/S0168-1923(00)00225-2)
- 512 Farrance, I., & Frenkel, R. (2012). *Uncertainty of Measurement: A Review of the Rules*
513 *for Calculating Uncertainty Components through Functional Relationships*. *The Clinical*
514 *Biochemist Reviews*, 33(2), 49–75.
- 515 Friedlingstein, P., O’Sullivan, M., Jones, M. W., Andrew, R. M., Hauck, J., Landschützer,
516 P., Le Quéré, C., Li, H., Luijkx, I. T., Olsen, A., Peters, G. P., Peters, W., Pongratz,
517 J., Schwingshackl, C., Sitch, S., Canadell, J. G., Ciais, P., Jackson, R. B., Alin, S. R., ...
518 Zeng, J. (2025). Global Carbon Budget 2024. *Earth System Science Data*, 17(3), 965–1039.

- 519 <https://doi.org/10.5194/essd-17-965-2025>
- 520 Hamdi, S., Moyano, F., Sall, S., Bernoux, M., & Chevallier, T. (2013). Synthesis analysis
521 of the temperature sensitivity of soil respiration from laboratory studies in relation to
522 incubation methods and soil conditions. *Soil Biology and Biochemistry*, 58, 115–126. <https://doi.org/10.1016/j.soilbio.2012.11.012>
- 524 Jackson, R. B., Lajtha, K., Crow, S. E., Hugelius, G., Kramer, M. G., & Piñeiro, G. (2017).
525 The Ecology of Soil Carbon: Pools, Vulnerabilities, and Biotic and Abiotic Controls.
526 *Annual Review of Ecology, Evolution and Systematics*, 48(Volume 48, 2017), 419–445.
527 <https://doi.org/10.1146/annurev-ecolsys-112414-054234>
- 528 Jian, J., Bailey, V., Dorheim, K., Konings, A. G., Hao, D., Shiklomanov, A. N., Snyder, A.,
529 Steele, M., Teramoto, M., Vargas, R., & Bond-Lamberty, B. (2022). Historically inconsis-
530 tent productivity and respiration fluxes in the global terrestrial carbon cycle. *Nature
531 Communications*, 13(1), 1733. <https://doi.org/10.1038/s41467-022-29391-5>
- 532 Jian, J., Vargas, R., Anderson-Teixeira, K., Stell, E., Herrmann, V., Horn, M., Kholod, N.,
533 Manzon, J., Marchesi, R., Paredes, D., & Bond-Lamberty, B. (2021). A restructured and
534 updated global soil respiration database (SRDB-V5). *Earth System Science Data*, 13(2),
535 255–267. <https://doi.org/10.5194/essd-13-255-2021>
- 536 Jiang, J., Feng, L., Hu, J., Liu, H., Zhu, C., Chen, B., & Chen, T. (2024). Global soil
537 respiration predictions with associated uncertainties from different spatio-temporal data
538 subsets. *Ecological Informatics*, 82, 102777. <https://doi.org/10.1016/j.ecoinf.2024.102777>
- 539 Jobbágy, E. G., & Jackson, R. B. (2000). The Vertical Distribution of Soil Organic Carbon
540 and its Relation to Climate and Vegetation. *Ecological Applications*, 10(2), 423–436. [https://doi.org/10.1890/1051-0761\(2000\)010%5B0423:TVDOSO%5D2.0.CO;2](https://doi.org/10.1890/1051-0761(2000)010%5B0423:TVDOSO%5D2.0.CO;2)
- 542 Jurasinski, G., Koebisch, F., Guenther, A., & Beetz, S. (2022). *Flux: Flux Rate Calculation
543 from Dynamic Closed Chamber Measurements*.
- 544 Liu, K., Li, X., Wang, S., & Zhang, H. (2023). A robust gap-filling approach for European

- 545 Space Agency Climate Change Initiative (ESA CCI) soil moisture integrating satellite
546 observations, model-driven knowledge, and spatiotemporal machine learning. *Hydrology*
547 and *Earth System Sciences*, 27(2), 577–598. <https://doi.org/10.5194/hess-27-577-2023>
- 548 Lunch, C., Laney, C., Mietkiewicz, N., Sokol, E., Cawley, K., & Network), N. (National. E. O.
549 (2025). *neonUtilities: Utilities for Working with NEON Data*.
- 550 Luo, Y., Ogle, K., Tucker, C., Fei, S., Gao, C., LaDeau, S., Clark, J. S., & Schimel, D. S. (2011).
551 Ecological forecasting and data assimilation in a data-rich era. *Ecological Applications*,
552 21(5), 1429–1442. <https://doi.org/10.1890/09-1275.1>
- 553 Maier, M., & Schack-Kirchner, H. (2014). Using the gradient method to determine soil gas
554 flux: A review. *Agricultural and Forest Meteorology*, 192–193, 78–95. <https://doi.org/10.1016/j.agrformet.2014.03.006>
- 555 Mariethoz, G., Linde, N., Jougnot, D., & Rezaee, H. (2015). Feature-preserving interpolation
556 and filtering of environmental time series. *Environmental Modelling & Software*, 72, 71–76.
557 <https://doi.org/10.1016/j.envsoft.2015.07.001>
- 558 Marshall, T. J. (1959). The Diffusion of Gases Through Porous Media. *Journal of Soil Science*,
559 10(1), 79–82. <https://doi.org/10.1111/j.1365-2389.1959.tb00667.x>
- 560 Millington, R. J., & Shearer, R. C. (1971). Diffusion in aggregated porous media. *Soil Science*,
561 111(6), 372–378.
- 562 Moffat, A. M., Papale, D., Reichstein, M., Hollinger, D. Y., Richardson, A. D., Barr, A. G.,
563 Beckstein, C., Braswell, B. H., Churkina, G., Desai, A. R., Falge, E., Gove, J. H., Heimann,
564 M., Hui, D., Jarvis, A. J., Kattge, J., Noormets, A., & Stauch, V. J. (2007). Comprehensive
565 comparison of gap-filling techniques for eddy covariance net carbon fluxes. *Agricultural and*
566 *Forest Meteorology*, 147(3), 209–232. <https://doi.org/10.1016/j.agrformet.2007.08.011>
- 567 Moldrup, P., Olesen, T., Yamaguchi, T., Schjønning, P., & Rolston, D. E. (1999). Modeling
568 diffusion and reaction in soils: 9. The Buckingham-Burdine-Campbell equation for gas
569 diffusivity in undisturbed soil. *Soil Science*, 164(2), 75.
- 570

- 571 NEON. (2024a). *Barometric pressure (DP1.00004.001)*. National Ecological Observatory
572 Network (NEON). <https://doi.org/10.48443/RT4V-KZ04>
- 573 NEON. (2024b). *Soil CO₂ concentration (DP1.00095.001)*. National Ecological Observatory
574 Network (NEON). <https://doi.org/10.48443/E7GR-6G94>
- 575 NEON. (2024c). *Soil physical and chemical properties, Megapit (DP1.00096.001)*. National
576 Ecological Observatory Network (NEON). <https://doi.org/10.48443/S6ND-Q840>
- 577 NEON. (2024d). *Soil temperature (DP1.00041.001)*. National Ecological Observatory Network
578 (NEON). <https://doi.org/10.48443/Q24X-PW21>
- 579 NEON. (2024e). *Soil water content and water salinity (DP1.00094.001)*. National Ecological
580 Observatory Network (NEON). <https://doi.org/10.48443/A8VY-Y813>
- 581 Norman, J. M., Kucharik, C. J., Gower, S. T., Baldocchi, D. D., Crill, P. M., Rayment, M.,
582 Savage, K., & Striegl, R. G. (1997). A comparison of six methods for measuring soil-
583 surface carbon dioxide fluxes. *Journal of Geophysical Research: Atmospheres*, 102(D24),
584 28771–28777. <https://doi.org/10.1029/97JD01440>
- 585 Pedersen, A. R. (2024). *HMR: Flux Estimation with Static Chamber Data*.
- 586 Phillips, C. L., Bond-Lamberty, B., Desai, A. R., Lavoie, M., Risk, D., Tang, J., Todd-Brown,
587 K., & Vargas, R. (2017). The value of soil respiration measurements for interpreting and
588 modeling terrestrial carbon cycling. *Plant and Soil*, 413(1), 1–25. <https://doi.org/10.1007/s11104-016-3084-x>
- 589
- 590 Raftery, A. E., Gneiting, T., Balabdaoui, F., & Polakowski, M. (2005). *Using Bayesian Model
591 Averaging to Calibrate Forecast Ensembles*. <https://doi.org/10.1175/MWR2906.1>
- 592 Rheault, K., Christiansen, J. R., & Larsen, K. S. (2024). goFlux: A user-friendly way to
593 calculate GHG fluxes yourself, regardless of user experience. *Journal of Open Source
594 Software*, 9(96), 6393. <https://doi.org/10.21105/joss.06393>
- 595 Sallam, A., Jury, W. A., & Letey, J. (1984). Measurement of Gas Diffusion Coefficient under
596 Relatively Low Air-filled Porosity. *Soil Science Society of America Journal*, 48(1), 3–6.

- 597 <https://doi.org/10.2136/sssaj1984.03615995004800010001x>
- 598 Shao, J., Zhou, X., Luo, Y., Li, B., Aurela, M., Billesbach, D., Blanken, P. D., Bracho, R.,
599 Chen, J., Fischer, M., Fu, Y., Gu, L., Han, S., He, Y., Kolb, T., Li, Y., Nagy, Z., Niu, S.,
600 Oechel, W. C., ... Zhang, J. (2015). Biotic and climatic controls on interannual variability
601 in carbon fluxes across terrestrial ecosystems. *Agricultural and Forest Meteorology*, 205,
602 11–22. <https://doi.org/10.1016/j.agrformet.2015.02.007>
- 603 Shao, P., Zeng, X., Moore, D. J. P., & Zeng, X. (2013). Soil microbial respiration from
604 observations and Earth System Models. *Environmental Research Letters*, 8(3), 034034.
605 <https://doi.org/10.1088/1748-9326/8/3/034034>
- 606 Sihi, D., Gerber, S., Inglett, P. W., & Inglett, K. S. (2016). Comparing models of microbial–
607 substrate interactions and their response to warming. *Biogeosciences*, 13(6), 1733–1752.
608 <https://doi.org/10.5194/bg-13-1733-2016>
- 609 Tang, J., Baldocchi, D. D., Qi, Y., & Xu, L. (2003). Assessing soil CO₂ efflux using continuous
610 measurements of CO₂ profiles in soils with small solid-state sensors. *Agricultural and Forest
611 Meteorology*, 118(3), 207–220. [https://doi.org/10.1016/S0168-1923\(03\)00112-6](https://doi.org/10.1016/S0168-1923(03)00112-6)
- 612 Tang, J., Misson, L., Gershenson, A., Cheng, W., & Goldstein, A. H. (2005). Continuous
613 measurements of soil respiration with and without roots in a ponderosa pine plantation
614 in the Sierra Nevada Mountains. *Agricultural and Forest Meteorology*, 132(3), 212–227.
615 <https://doi.org/10.1016/j.agrformet.2005.07.011>
- 616 Taylor, J. R. (2022). *An Introduction to Error Analysis: The Study of Uncertainties in Physical
617 Measurements, Third Edition* (3rd ed.). University Science Press.
- 618 Wilson, S. J., Bond-Lamberty, B., Noyce, G., Bittencourt Peixoto, R., & Megonigal, J. P.
619 (2024). Fluxfinder: An R Package for Reproducible Calculation and Initial Processing of
620 Greenhouse Gas Fluxes From Static Chamber Measurements. *Journal of Geophysical Re-
621 search: Biogeosciences*, 129(11), e2024JG008208. <https://doi.org/10.1029/2024JG008208>
- 622 Yan, Z., Bond-Lamberty, B., Todd-Brown, K. E., Bailey, V. L., Li, S., Liu, C., & Liu, C. (2018).

- 623 A moisture function of soil heterotrophic respiration that incorporates microscale processes.
- 624 *Nature Communications*, 9(1), 2562. <https://doi.org/10.1038/s41467-018-04971-6>
- 625 Yan, Z., Liu, C., Todd-Brown, K. E., Liu, Y., Bond-Lamberty, B., & Bailey, V. L. (2016).
- 626 Pore-scale investigation on the response of heterotrophic respiration to moisture conditions
- 627 in heterogeneous soils. *Biogeochemistry*, 131(1), 121–134. <https://doi.org/10.1007/s10533-016-0270-0>
- 628
- 629 Zhang, R., Kim, S., Kim, H., Fang, B., Sharma, A., & Lakshmi, V. (2023). Temporal
- 630 Gap-Filling of 12-Hourly SMAP Soil Moisture Over the CONUS Using Water Balance
- 631 Budgeting. *Water Resources Research*, 59(12), e2023WR034457. <https://doi.org/10.1029/2023WR034457>
- 632
- 633 Zhao, J. (2019). FluxCalR: A R package for calculating CO₂ and CH₄ fluxes from static
- 634 chambers. *Journal of Open Source Software*, 4(43), 1751. <https://doi.org/10.21105/joss.01751>
- 635
- 636 Zobitz, J., Ayres, E., O'Rourke, K., Werbin, Z., Lee, L., Abdi, R., Mehmeti, D., & Xiong, L.
- 637 (2024). *neonSoilFlux: Compute Soil Carbon Fluxes for the National Ecological Observatory*
- 638 *Network Sites*.
- 639 Zobitz, J., & Zimmerman, N. (2025). *Supporting Code and Data for neonSoilFlux: An R*
- 640 *Package for Continuous Sensor-Based Estimation of Soil CO₂ Fluxes*. Zenodo. <https://doi.org/10.5281/zenodo.17516320>
- 641